

Your thesaurus codes are:

03(02.13.2; 11.09.1 NGC 4449; 11.13.2)

Modeling of magnetic field structures in irregular galaxies of Magellanic type

K. Otmianowska-Mazur¹, K.T. Chyży¹, M. Soida¹, and S. von Linden²

¹ Astronomical Observatory, Jagiellonian University, ul. Orła 171, 30-244 Kraków, Poland

² Landessternwarte Heildelberg, Königstuhl, 69117 Heidelberg, Germany

Received 18 June 1999 / Accepted 26 April 2000

Abstract. The recently observed strong-regular magnetic fields in the dwarf irregular (IBm) galaxy NGC 4449 are not predicted by classical turbulent dynamo theory. The very slow and almost unorganized rotation of the galaxy appears to contradict the observed large-scale magnetic fields manifested in a fan-like structure emanating from vigorous star formation in the central part of the galaxy and a spiral shell-like pattern on its periphery. In this paper, we investigate the influence of different physical processes on the evolution of magnetic fields. We invoke a model of an irregular galaxy by numerically solving the kinematic dynamo equation and adopting a gas velocity field obtained from N-body simulations. We report that the puzzling magnetic fragments of a polarized shell containing spiral magnetic fields in NGC 4449 can originate from shear motions of the interstellar gas associated with a bar perturbation. A significant role, recently postulated “fast” dynamo action, is needed to maintain the high magnetic energy in the presence of a turbulent diffusion. To model the observed magnetic fields in the central part of NGC 4449 we incorporate high stellar activity (observed within the main body of the galaxy) as a source of random magnetic fields. Additionally, we include a spherical outflow to reproduce the radially oriented “fans” of magnetic field that are observed. The inclusion of this outflow, however, does not lead to the observed radio polarization properties and the magnetic pitch angle distribution in the central part of the galaxy, so a more realistic model of an outflow with regard to the star formation distribution, is needed.

Key words: Magnetohydrodynamics (MHD) – galaxies: individual: NGC 4449 – galaxies: magnetic fields

1. Introduction

The origin of large-scale magnetic fields, widely observed in rapidly and differentially rotating spiral galaxies (Ruzmaikin et al. 1988), is usually explained by a well-known process of a magnetohydrodynamical (MHD) dynamo (e.g. Elstner et al. 1998). This mechanism is associated with small-scale phenomena from turbulent motions (Elstner et al. 1992) influenced by

the differential rotation present in a galactic disk. In very slow and nearly rigidly rotating dwarf irregulars (dIrrs), the presence of well organized magnetic field structures has not yet been predicted. The “classical” dynamo mechanisms required to produce global magnetic fields are ineffective in disks rotating with velocities an order of magnitude less than those found in normal spiral and barred galaxies. Despite this, significant magnetic fields were found in two dwarf irregulars: the Large Magellanic Cloud (LMC) and the Magellanic-type NGC 4449. In the first of them patchy structures of the magnetic field with a weak indication of a large-scale organization were observed (Klein et al. 1993). Using the Effelsberg radio telescope, Klein et al. (1996) reported the first detection of magnetic fields running across the galaxy NGC 4449. Recent observations of NGC 4449 (Chyży et al. 2000), utilizing the high resolution and sensitivity VLA data, indicate the presence of strong large-scale magnetic fields that form radial “fans” in the central region and puzzling fragments of a spiral shell-like structure at its periphery (see Fig. 3d). The strength of these observed regular fields is about $9 \mu\text{G}$, comparable to the magnitude found in the spiral galaxies.

Keeping in mind the above facts, the outstanding problem is what kind of physical mechanism could be responsible for producing the observed large-scale magnetic configuration in the galaxy. We need a faster process which is much more efficient than the “classical” turbulent dynamo. The solution to the problem was proposed by the “fast dynamo” theory (Parker 1992) taking into account Parker instabilities, cosmic rays and magnetic reconnections. A new fast dynamo model based on the Parker hypothesis was constructed by Hanasz & Lesch (1997, 1998) where the existence of flux tubes interactions was introduced. The term “fast dynamo” refers to dynamos in which the generation rate of the mean magnetic field remains finite in the limit of vanishing resistivity. This mechanism allows the possibility of introducing a large α value in the presence of a weak magnetic field and of a high star formation activity (Hanasz & Lesch 1997), which gives an excess of cosmic ray pressure over the magnetic pressure. The “fast dynamo” model can explain the existence of strong magnetic fields in young blue objects, i.e. excessively star-bursting galaxies (Hanasz & Lesch 1997).

Herein we present five MHD numerical scenarios as an attempt to explain the origin of the observed magnetic fields in

Send offprint requests to: K. Otmianowska-Mazur

Correspondence to: otmian@oa.uj.edu.pl

irregular galaxies. As a seed field for our model we introduced A0 modes which are expected as dynamo solutions for slowly and almost rigidly rotating bodies, e.g. in central regions of spiral galaxies (Ruzmaikin et al. 1988). The numerical models involving the S0 mode, which we tested as well, result in magnetic fields structures possessing a strong B_r component in the disk plane – too high in comparison with observations.

We analyze mainly NGC 4449 since its magnetic fields have been the most extensively studied, however the LMC case is discussed as well. NGC 4449 is a dwarf galaxy belonging to LMC class of irregulars possessing a bar similar in size and mass to the LMC (Bajaja et al. 1994). Because of its proximity, this galaxy was extensively studied in many bands. Basic parameters are summarized in Table 1. NGC 4449 is a galaxy with moderate star formation activity, producing long filaments and a frothy structure of the warm (10^4 K) ionized interstellar medium (Bomans et al. 1997, Hunter & Gallagher 1990 and 1992). The hot gas was also found in active star-forming regions and in outflows from them (Bomans et al. 1997). According to $H\alpha$ study (Hill 1994), the period of a high star formation activity occurring mainly in the bar, passed about 5–6 Myr ago. Presently, vigorous star formation is concentrated in the northern part of the stellar bar which is rich in HII regions, blue super-giants and very young supernova remnants.

The galaxy is situated in a huge gaseous halo (van Woerden et al. 1975, Bajaja et al. 1994, Hunter et al. 1998) that has a diameter about 14 times larger than the optical extent of the galaxy (see Table 1). This halo counter-rotates relative to the inner part of the galaxy. The observed S-shaped morphology of the HI envelope most likely suggests a gravitational interaction with another body e.g. the companion dwarf galaxy DDO125 (Hunter et al. 1998). This provides evidence of the interpretation that the dynamical age of prominent features in the gas flow is of the order of 10^8 yr (Hartmann et al. 1986). Stemming from its dynamical history, the complexity of the stellar and gas kinematics has thus far prevented the construction of a detailed rotation curve of NGC 4449.

The existing rotational star and ionized gas velocity studies (Sabbadin et al. 1984, Hartmann et al. 1986) indicate that the galaxy slowly rotates (in the opposite direction to the HI halo) with a maximum velocity of about 20–30 km s^{-1} . The analysis of HII and HI data shows a rather complicated velocity field, with discontinuities along the major axis and large dispersion along the minor axis (see Hartmann et al. 1986, Chyży et al. 2000). External causes, e.g. a merger or a past interaction with another system, can explain these complexities. The case of LMC is different as it shows obvious evidence of ongoing interaction. In fact, it orbits around the Milky Way and is getting compressed at the leading edge. The relative speed between LMC and the Galaxy halo is supersonic (about 465 km s^{-1}) which causes 10 times enhancement of the gas pressure and creates a bow-shock in the compression region (de Boer et al. 1998). Huge star formation complexes (including 30 Doradus) are probably shock-induced in this (SE) part of the galaxy where the highest radio polarization emission is also observed.

Table 1. Basic properties of NGC 4449

Type	IBm	LEDA
R.A. (2000)	$12^{\text{h}}28^{\text{m}}11^{\text{s}}.3$	LEDA
Decl. (2000)	$44^{\circ}5'30''$	LEDA
Optical extent	$4.7' \times 3'$	de Vaucouleurs et al. (1976)
HI extent	$70' \times 65'$	Bajaja et al. (1994)
Inclination	43°	Tully (1998♣)
Position angle	45°	LEDA database
Distance	3.7 Mpc	Bajaja et al. (1994)
Abs. B -magn.	−18.4	de Vaucouleurs et al. (1991)
M_{tot}	$7 \cdot 10^{10} M_{\odot}$	Bajaja et al. (1994)
M_{HI}	$2.3 \cdot 10^9 M_{\odot}$	Bajaja et al. (1994)

To simulate magnetic field evolution in the Magellanic-type irregulars we apply an interstellar gas flow having a small, but realistically feasible, value of rotational velocity with significant gradients and a bar-like disturbance. We then kinematically solve the dynamo equation using a (three-dimensional) MHD numerical simulation. Five different models are used to analyze the importance of dynamo action, galactic outflow, and additional sources of a random magnetic component. We introduce distributions of relativistic electrons within the model to compute maps of polarized radio emission. Modeled distributions of polarized synchrotron radiation and magnetic field configuration are compared to radio observations of NGC 4449. From these studies we conclude:

1. the large-scale polarized fragments of a spiral shell-like structure observed in NGC 4449 can be substantially explained by a gas flow around the galaxy bar and a fast dynamo mechanism;
2. the approximate level of magnetic energy could be maintained by both processes: the dynamo action and the input of chaotic magnetic fields;
3. the observed “fan-like” structure of the magnetic field and the large-scale shell with spiral magnetic pattern cannot be reproduced by pure outflow and wind phenomena, stretching and compressing passively random magnetic fields, produced in the strongly star forming center of NGC 4449.

We describe these findings in Sects. 2 through 6 as follows: Sect. 2 summarizes the radio observations of NGC 4449, Sect. 3 outlines the construction of the numerical model used to simulate NGC 4449, Sect. 4 details the model input parameters and describes five variants of the modeling effort, Sect. 5 reports the results of model matching to observation, and the concluding discussion is in Sect. 6.

2. Radio emission of NGC 4449

The high resolution and sensitivity radio continuum observations of NGC 4449 by Chyży et al. (2000) were obtained using the VLA interferometer in its most compact D -configuration at 8.46 GHz and 4.86 GHz. To minimize the loss of extended smooth structure, the total power and linear polarization maps were combined with data from the single-dish Effelsberg radio

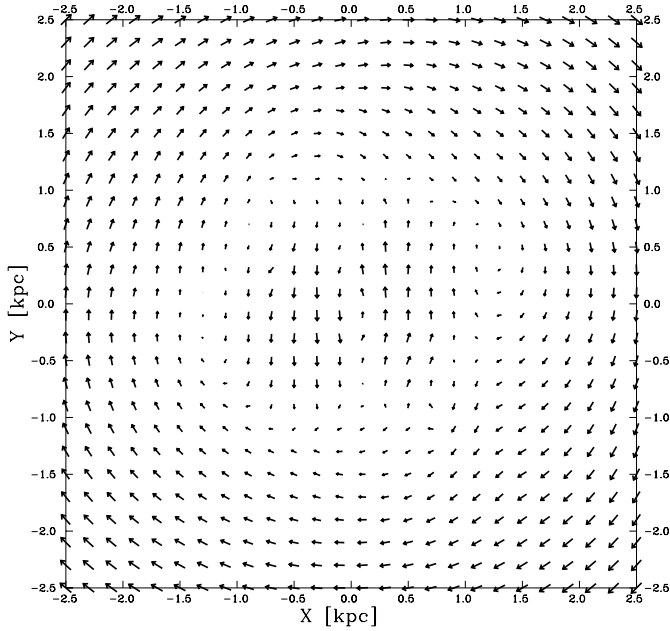


Fig. 1. Vector plot of the gas flow velocity field in the galactic plane. The corotation velocity of the gas flow with the bar (18 km/h/kpc) is subtracted for better presentation of gas flow kinematical properties.

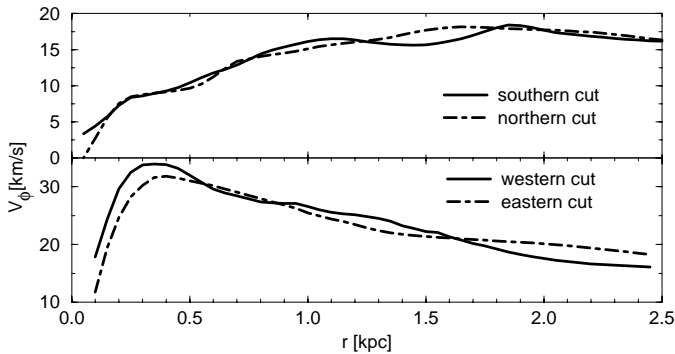


Fig. 2. The rotation curves of the model galaxy, calculated from the velocity field used for computations along four semi-axes (northern & southern cut, upper panel) and across (eastern & western cut, bottom panel) the bar.

telescope. The total power radio emission at both frequencies (see Figs. 1 and 3 in Chyży et al. 2000) shows close connection to the $H\alpha$ emission. Strong radio peaks coincide spatially with bright star-forming regions. In these regions, the thermal fraction locally attains as much as 70%. Diffuse nonthermal emission is seen far away from the galaxy star-forming body, extending up to 2 optical radii. However, a few faint peaks at positions corresponding to separate active star formation regions are also observed in these distant regions. Since the total power radio emission is significantly confused by the thermal component near these regions, it will not be a subject of our modeling.

A radio polarization intensity (PI) contour map, obtained at 4.86 GHz, as well as the corresponding magnetic field vectors, are overlaid onto an optical image of NGC 4449 in Fig. 3d. The orientation of magnetic fields are not corrected for the effect of

Faraday rotation which is generally not strong, giving average rotation measures of 50 rad/m^2 and only locally reaching about 200 rad/m^2 (corresponding to rotation of magnetic field vectors by 8° and 30° , respectively). Magnetic vectors show two distinct kinds of structures (see Chyży et al. 2000 for more details). Near the central region of the galactic disk these are directed nearly radially outwards, forming polarized “fans” co-aligned with the system of elongated $H\alpha$ filaments (Bomans et al. 1997). Thus the orientation of the B -vectors are probably closely associated with large-scale gas dynamics around star-active regions.

The second structure is a well organized and coherent pattern of magnetic vectors surrounding the galaxy from the north-east through west to the south-west, forming a kind of shell of polarized emission (see Fig. 3d). The degree of polarization in this shell structure reaches 50% near the brightest peaks.

The analysis of the distribution of the Faraday rotation measurements reveals large-scale unidirectional magnetic fields, both in fans and in the ridge, providing evidence of genuine galaxy-scale regular fields. These structures cannot be explained solely by squeezed or stretched random fields resulting from strong galactic winds or shocks (Chyży et al. 2000). The estimated mean equipartition value of regular fields reaches peak values of about $9 \mu\text{G}$ in the polarized ridge and $7 \mu\text{G}$ in the western fan. The total field in these regions amounts to about $15 \mu\text{G}$, a value comparable to that in bright spiral galaxies. The polarized shell coincides well with a similar structure in HI emission (Fig. 4 in Chyży et al. 2000) and even the brightest peaks in both distributions lie close to each other. It is possible to reconcile this observation with a postulated global flow of gas around the galactic bar and in the halo.

The polarized emission and magnetic field structure observed at 4.86 GHz are used as the main observational target for our modeling. At this frequency, magnetic pitch angles can be locally affected by the Faraday rotation but the polarization map is more sensitive than the higher frequency (8.46 GHz) one (compare Figs. 2 and 4 in Chyży et al. 2000) and hence more suitable for the modeling.

3. Model construction

NGC 4449 is morphologically similar to LMC: both galaxies possess a bar-like structure in the central part of the disk. The rotation pattern of LMC is well known (e.g. Luks & Rohlfs 1992 and the review paper given by Westerlund 1990). For the main disk component it is linear for galactic radii smaller than 0.7 kpc and flattens for the radii greater than 1.4 kpc (Luks & Rohlfs 1992). The maximum rotational velocity value is about 50 km s^{-1} , a value comparable with the maximum of about 30 km s^{-1} for NGC 4449 (Chyży et al. 2000). However, the velocity field in the aforementioned galaxy is certainly more complicated than in LMC, explained partially by at least two processes: a shear flow around the bar (with substantial velocity gradients) and the radial outflow (wind) connected with the high star formation rate in the main body of the galaxy (Bomans et al. 1997). Both components are applied in our model. In the case of LMC, apart from the above mentioned disk component, about

20% of HI gas was found in two large complexes at lower radial velocities situated about 50–500 pc above the disk in the direction towards the Galaxy (Luks & Rohlfs 1992). The starburst region 30 Dor is partly sitting in one (SE) of these features. The relation between the bar and these lower velocity components is unclear.

In our experiment we adopt a gas velocity field resulting from the N-body simulations of a galactic dynamics (Otmianowska-Mazur et al. 1997). The model consists of two essential components: a collisionless self-gravitating disk composed of stars, and colliding molecular clouds (highly inelastic clouds) moving in the gravitational potential of the stellar population. It is also necessary to analytically add a contribution from the bulge and dark matter halo (see Otmianowska-Mazur et al. 1997 for details). In our model the molecular clouds are assumed to represent the large scale velocity field of the gas, controlling the magnetic field evolution. In our present experiment we adopt one velocity field ($t = 9.1 \times 10^8$ yr) resultant from the calculations shown in Otmianowska-Mazur et al. (1997) as model II. The chosen distribution of molecular clouds (Fig. 3a, grey plot) is morphologically similar to the bar-like structure present in NGC 4449 (see Figs. 3d and 5d, grey plots). As we demonstrate, the galaxy model shows only a bar in the central part of its disk with almost no evidence of spiral arms. The value of rotational velocity in this model is about 300 km s^{-1} which is one order of magnitude too high for our dwarf galaxy. Therefore we decimate the entire velocity field. We also decreased the linear scale by 6.0. The rescaling was performed conforming the virial theorem. The modeled galaxy possesses a radius of about 2.5 kpc and rotational velocities with maxima of about 30 km s^{-1} (see Fig. 2). The resulting velocity field vectors shown in co-rotating coordinates are presented in Fig. 1. The shear in the flow of gas around the bar structure is clearly visible. Fig. 2 presents four rotation curves showing the axisymmetric linear velocity component v_ϕ along the bar (upper panel) and perpendicular to it (lower panel). The first case predominantly shows signs of rigid rotation (up to $r < 1.25\text{--}1.5$ kpc), presenting a quite large velocity dispersion, as well. In the direction perpendicular to the bar, rigid rotation is only for $r < 0.3$ kpc and further differential rotation with significant velocity gradient is clearly seen.

The resultant velocity field is used to numerically solve the dynamo equation in the following form:

$$\partial \mathbf{B} / \partial t = \text{rot}(\mathbf{v} \times \mathbf{B}) + \text{rot}(\alpha \mathbf{B}) - \text{rot}(\eta \text{rot} \mathbf{B}) \quad (1)$$

where \mathbf{B} is the magnetic induction, \mathbf{v} is the velocity field of the gas, α is the dynamo coefficient describing the mean helicity of turbulent motions and η is the turbulent dynamo coefficient. The calculations are performed with the three-dimensional (3D) finite difference code, ZEUS3D, (Stone & Norman 1992) in rectangular coordinates with inclusion of the α -effect as a source term.

We presuppose that the relativistic electron number density distribution decreases exponentially in the model galaxy with radius and height, possessing the scale of 4.0 kpc and 1.5 kpc, respectively. The maps of Stokes parameters I, Q and U (in arbitrary units) are calculated by integrating the transfer equa-

Table 2. Input parameters for MHD models

Model	I	II	III	IV	V
scale lengths [kpc]:					
grid step in X and Y:	0.05	0.05	0.05	0.05	0.05
grid step in Z:	0.08	0.08	0.08	0.08	0.08
number of grid points					
– in X and Y:	101	101	101	101	101
– in Z:	51	51	51	51	51
$\alpha_{xx} = \alpha_{yy} = \alpha_{zz}$ [km s^{-1}]:	0	5	5	5	0
η [$10^{26} \text{ cm}^2 \text{ s}^{-1}$]:	1.5	1.5	1.5	1.5	1.5
outflow speed [km s^{-1}]:	0	0	50	50	50
random field:	no	no	no	yes	yes

tion along the line of sight. Volume elements are taken small enough to assume uniform magnetic field inside, and constant intrinsic polarization degree and a synchrotron emissivity (e.g. Pacholczyk 1970). The position and orientation on the sky of our modeled galaxy is the same as the galaxy NGC 4449 itself. We assume that the position angle of the modeled bar is determined by the observed H α emission structure (Fig. 5d), nearby recent star formation regions. For comparison with observations, the resulting maps are convolved with the $19''$ Gaussian beam and combined together to obtain polarization intensity and polarization position angle maps. All Faraday effects are neglected except model IV.

4. Model input parameters

We performed our simulations in five basic experiments — I, II, III, IV and V for which the input parameters are summarized in Table 2. In all models we use 101 grid points in the X and Y directions and 51 in vertical one. The distance between grid points along the X and Y axis is 50 pc yielding 5 kpc as the diameter of the modeled galaxy. Along the Z axis the step is 80 pc, which gives 4 kpc as our irregular galaxy vertical size. According to the study of gas and stars motions, the observed features in the galactic velocity field cannot be maintained for time scales longer than a few 10^8 yrs (Hartmann et al. 1986). For this reason our computations are performed mainly for 5.0×10^8 yr. The time step used in these calculations is 0.5×10^5 yr.

The initial configuration of the magnetic field possesses a circular structure (only the B_ϕ component is present, which decreases exponentially with a coefficient for radial decay of 1.8 kpc, and vertical decay of 0.8 kpc), with the mean value about $1 \mu\text{G}$, a few times smaller than the maximum value given from observations of NGC 4449 (Chyży et al. 2000). It is highly probable that in the past, before a probable close encounter with another galaxy, NGC 4449 possessed a larger gaseous disk with faster rotation than today. The dynamo could work efficiently under those conditions and could produce axisymmetric magnetic fields similar to the ones used as inputs in our calculations.

The presence of both dynamo coefficients α and η in our model is supported by H α observations of NGC 4449 (Bomans et al. 1997) that show a large number of star formation regions. The first coefficient describes the amplification term in the dy-

namo Eq. (1) and has a tensorial form. We assign to it a positive constant value of 5 km s^{-1} for all three components, which is expected for A0 modes. Such a large value of α is in agreement with the value obtained from the fast dynamo model (Hanasz 1997 and is understandable due to a high star formation activity of NGC 4449 providing the observed r.m.s. velocity about 20 km s^{-1} over 1 kpc (Hartmann et al. 1986). The turbulent motions activated by the above mentioned processes enable us to assume a typical value of the second dynamo coefficient, the diffusivity $\eta = 1.5 \cdot 10^{26} \text{ cm}^2 \text{ s}^{-1}$, which is also estimated by the fast dynamo theory (Hanasz, 1997). The classical dynamo mechanism gives the same range of the dynamo coefficients, however, on much longer time scales. To test the influence of both dynamo coefficients, we performed simulation I with turbulent diffusion only, while in experiment II we additionally accounted for the α -effect (see Table 2). The assumption of non-linear feedback is introduced only via “ α -quenching”, where $\alpha \propto B^{-2}$ (see e.g. Rädler & Wiedemann 1989).

In the central region of NGC 4449 a radial outflow of warm gas is observed in $\text{H}\alpha$ emission in a form of a large number of different shaped filaments, extending from the bar (Bomans et al. 1997). This outflow displays strong stellar winds and supernova blasts from active star-forming regions concentrated within a bar-like structure. Therefore in our next experiment (model III, Table 2) we add an outflow of gas from the center of the modeled galaxy. The assumed distribution of the outflow is spherical, being the simplest approximation of the problem. A similar outflow was analyzed by Brandenburg et al. (1993) in a magnetic field study of a spiral galaxy NGC 4631, however the actual wind has a more local character. We adopt 50 km s^{-1} as the maximum value of its velocity, which is in good agreement with the Alfvén speed calculated for mixture of thermal gas (hydrogen) and cosmic-ray gas (CR) (Pohl & Schlickeiser 1990) (see Table 2), although even higher values seem to be acceptable (Bomans et al. 1997, Breitschwerdt et al. 1991). The modeled outflow decreases exponentially from the radius of 250 pc with a characteristic scale of 0.6 kpc. This fact is connected with the assumed local character of the above mentioned processes. For temperatures of the hot interstellar medium (HIM) (below a million degrees), radiative cooling prevents continuous mass loss by a global wind on scales of a whole galaxy (Breitschwerdt et al. 1991). The second mechanism preventing the formation of wind is a high intergalactic pressure possibly present in the HI cloud surrounding NGC 4449 (see Table 1, Breitschwerdt et al. 1991). The more physical model of an outflow with regard to the star formation distribution is in preparation.

Model IV (see Table 2) combines all the above-mentioned processes and an additional mechanism of the build-up of a random turbulent magnetic field in the central part of the modeled galaxy. Every 10^7 yr and at every grid point, three magnetic components (B_x , B_y and B_z) are added chaotically, possessing a total mean value about $0.1 \mu\text{G}$. Such a field can be easily provided by a stellar activity present in the observed galaxy within its bar. In our Galaxy the estimations of a magnetic field ejections from young hot stars and supernova explosions give the magnetic field of average strength of a few μG (Ruzmaikin et

al. 1988). The modeled random field is distributed spherically and diminishes in the same manner as the outflow in model III.

Model V tests the possibility that the observed magnetic structure could be created without the dynamo action ($\alpha = 0$, see Table 2), but only by the outflow and the chaotic magnetic field from the center of the galaxy. The assumed averaged strength of this field is $0.5 \mu\text{G}$.

5. Results

Model I illustrates the influence of a pure velocity field and diffusion on an initially uniformly distributed circular magnetic field in the absence of a dynamo process and galactic wind. Fig. 3a presents the magnetic field vectors in the galactic plane with time step $t = 1.3 \times 10^8$ yr superimposed on the gas density greyscale plot. The modeled distribution of gas displays general character of the observed bar structure visible in the optical picture of NGC 4449 (Fig. 3d, greyscale plot). In Fig. 3c the modeled bar is presented (in greys) as a projection onto the sky plane. The detailed comparison of the distribution of the modeled gas with the optical picture is not entirely justifiable because the latter shows mainly a stellar component of the galaxy, while the model shows molecular clouds which are more closely connected to the interstellar medium. Our bar is then closer to the pattern observed in the $\text{H}\alpha$ emission (Fig. 5d, greyscale plots). The existence of velocity shearing around the bar and in the disk first produces weak, but later clearly visible ring-like distributions of magnetic fields (Fig. 3a), as well as a weak extension on the western side of the bar. The resultant toroidal intensity structure (better visible as a grey plot in Fig. 3b) appears in the region where the gas flow goes around the bar and has the strongest shear. In fact, in Fig. 1, the velocity vectors going from the southern end of the bar are distributed around it (v_r is positive, see Fig. 3b topolines). Next, they go onto the left side of the bar, parallel to its main axis (the magnitude of v_r decreases and vector changes its direction). Near the northern end the vectors start to go around it, inclining again to the center with a negative (this time) radial component. On the right side the situation is similar. At the bar top we can see a small inflow of the gas from the north direction (the radial component is negative in that area, see Fig. 3b), causing the visible maximum of magnetic strength (Fig. 3b). Such velocity patterns are normally expected for gas flows around bars (Athanasoula 1992). In the presence of magnetic field and diffusion, the fast changes of a radial velocity sign cause a quick decrease of a magnetic energy inside the ring. The minimum of the magnetic intensity present at the bottom of the bar on its right side is probably caused by small velocity irregularities visible in this region in Fig. 1, decreasing locally the velocity shear.

The map of a polarized emission constructed from the actual magnetic configuration is presented in Fig. 3c. Due to the integration and projection effects, the original sharp magnetic field distribution is no longer visible. The resulted magnetic structure is much thicker and the polarized intensity map does not possess isolated regions, having three maxima distributed around the center. The magnetic vectors are inclined to the bar at a small

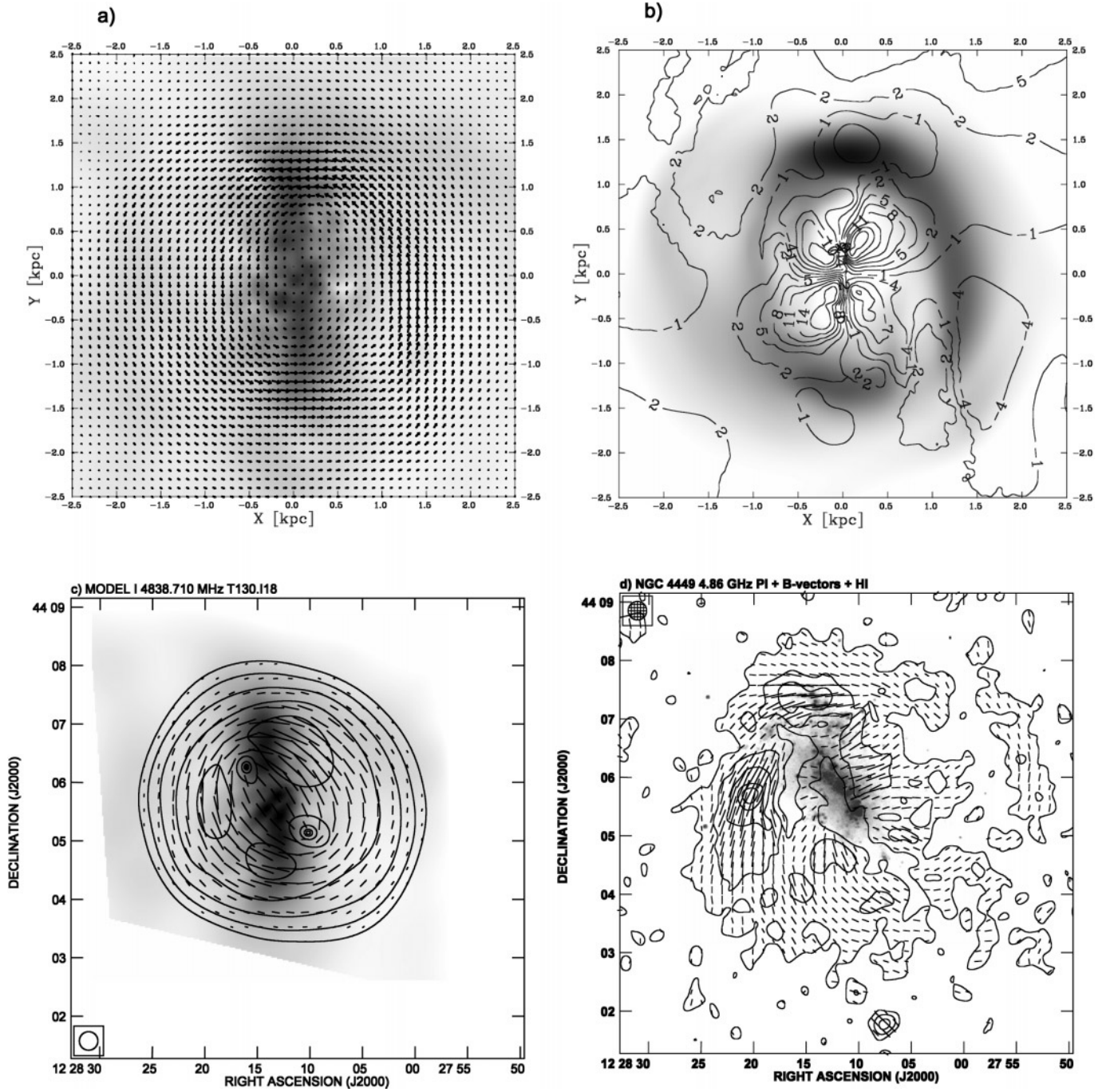


Fig. 3. **a** Magnetic field vectors of model I in the galactic plane at $t = 1.3 \cdot 10^8$ yr superimposed onto a molecular clouds density distribution (grey plot); **b** Contour plot of the radial velocity component superimposed onto magnetic field intensity of model I at the same time step; **c** Contour plot of polarized intensity (in arbitrary units) with polarization B-vectors of model I, overlaid onto clouds density integrated along the line of sight, all projected onto the sky plane with inclination and position angle same as NGC 4449; **d** The contours of PI of NGC 4449 at 4.86 GHz with polarization B-vectors superimposed onto an optical image. The contour levels are (3, 10, 20, 30, 35) $5.4 \cdot 10^{-5}$ Jy/b.a..

angle and two minima of emission are visible at both bar ends. Such structures are normally observed for barred galaxies due to beam depolarization effect. In order to compare our modeled map with observations, Fig. 3d shows the polarized emission of NGC 4449 (4.86 GHz) superimposed onto the optical picture of this galaxy as a greyscale plot. At this stage of the modeling,

the resultant pitch angle of magnetic vectors is smaller than in the real galaxy and the emission map fills the whole central part of the disk in the opposition to the observations.

The calculation of model II (see Table 2) combines the above described processes (velocity shears and the turbulent diffusion) with the presence of the dynamo mechanism (a non zero

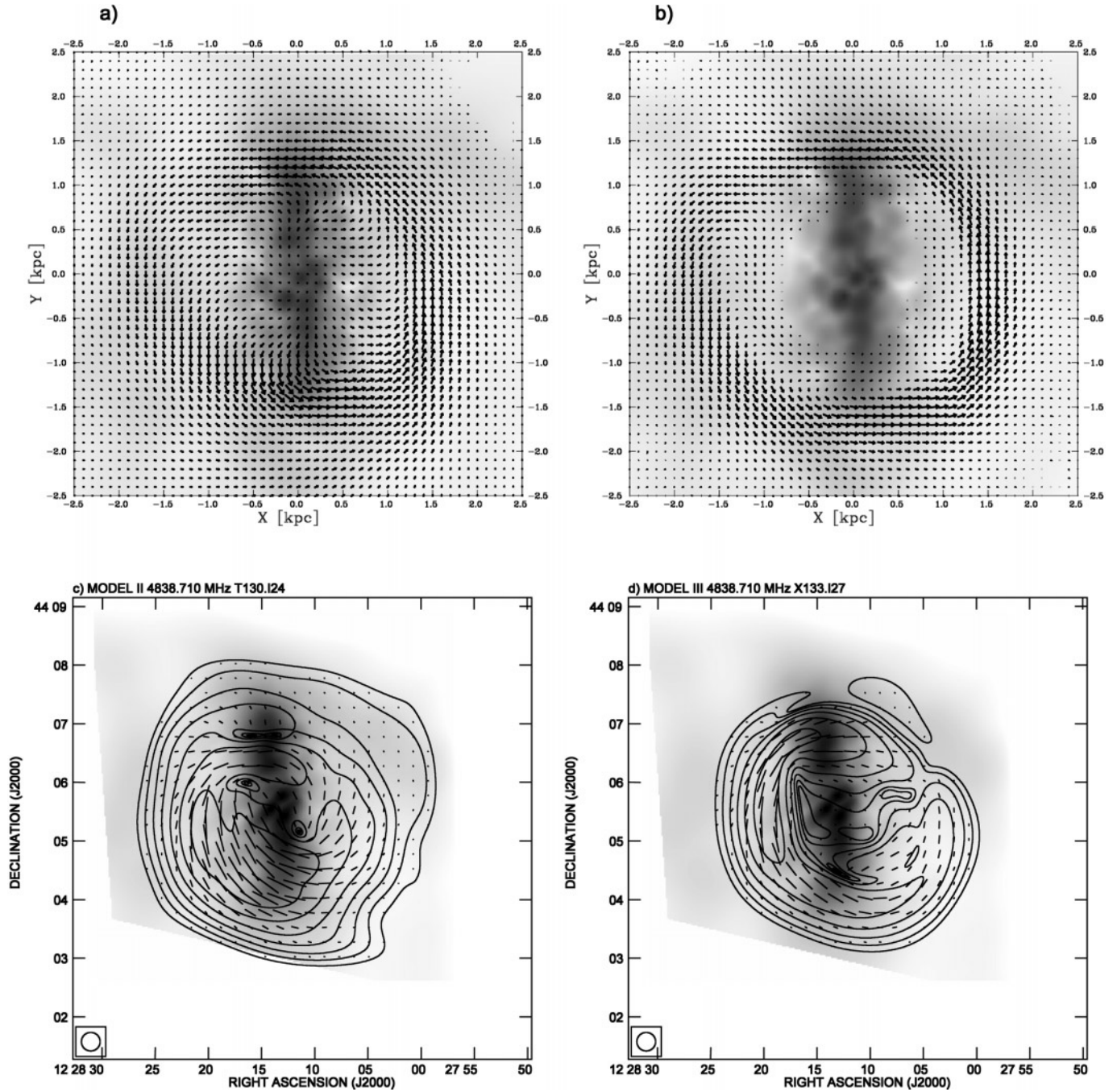


Fig. 4. **a** and **b** Magnetic field vectors of model II and III in the galactic plane superimposed onto molecular clouds density at $t = 1.3 \cdot 10^8$ yr; **c** and **d** Contour plot of polarized intensity (in arbitrary units) with polarization B-vectors of model II and III respectively, overlaid onto clouds density integrated along the line of sight at the same time step.

α -effect). In comparison with model I, the resultant magnetic structure (Fig. 4a) is less uniform but the spiral-like pattern is much more clearly visible. We can see the magnetic intensity maximum at the top and bottom of the bar (caused by velocity shear around the bar along with gas inflow from the north direction). Due to the α -effect the vector pitch angles are much higher, better resembling the observation (Fig. 3d) than the results of experiment I. The α -effect, although uniform, influences the magnetic field not only by increasing its total energy (see

Fig. 6), but also by changing the entire magnetic configuration. Firstly, the A0 mode appears very quickly during the simulation (as it is expected for the fast dynamo action) and magnetic lines form helical structures going around the Z-axis and then high in the direction perpendicular to the galactic plane. This effect reorganizes the magnetic distribution obtained from model I (Fig. 3a). Fig. 4c presents a spiral-like structure of magnetic vectors, obtained from the polarization emission model. The PI contour map exhibits only one maximum on the left-bottom side

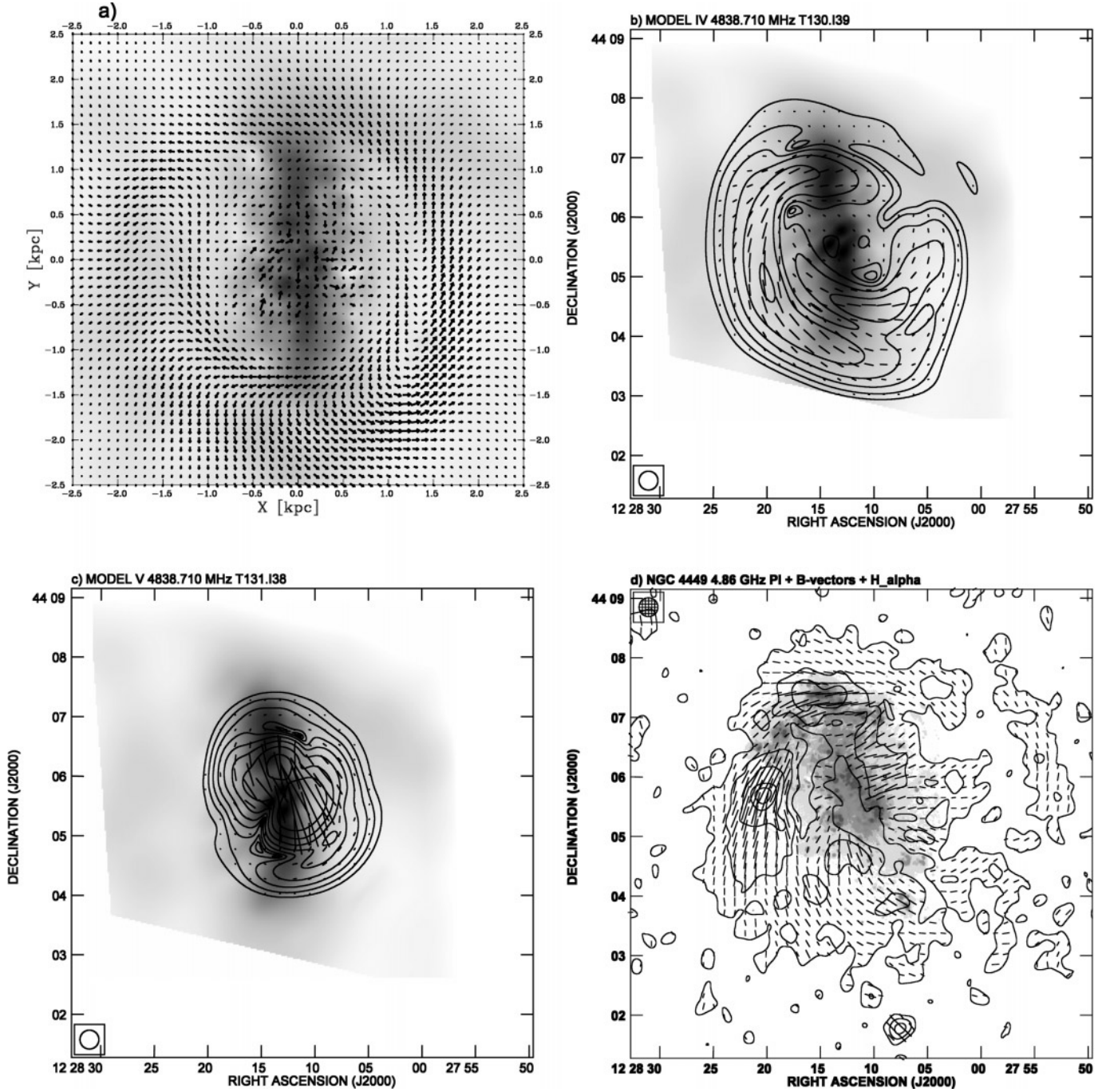


Fig. 5. **a** Magnetic field vectors of model IV in the galactic plane superimposed onto molecular clouds density at $t = 1.3 \cdot 10^8$ yr; **b** and **c** Contour plot of PI (arbitrary units) with polarization B-vectors of model IV (at $t = 1.3 \cdot 10^8$ yr) and V (at $t = 9.0 \cdot 10^8$ yr), overlaid onto clouds density integrated along the line of sight, all projected onto the sky plane with inclination and position angle same as NGC 4449; **d** The same as in Fig. 3d but overlaid onto the $H\alpha$ image from Bomans et al. (1997).

of the bar and the small central region of depolarized emission. Now, the magnetic structure is more similar to observations (Fig. 3d) than the results of experiment I.

Model III (see Table 2) preserves all mechanisms of model II, but includes the presence of a spherical outflow blowing outward from the central region of the modeled galactic disk with a maximum velocity of 50 km s^{-1} . The resultant mag-

netic field (Fig. 4b) displays a strong toroidal magnetic pattern having, however, small deviations from axisymmetrical distribution. The maximum of magnetic field strength is observed on the south-eastern side of the bar. The additional velocity shear connected with the assumed fast diminishing of a wind flow at $r=1$ kpc increases the resultant magnetic field strength in the shell-like region in comparison with two earlier models. This

finding is illustrated by the highest growth of the total magnetic energy E normalized to its initial value, shown in Fig. 6 for this model. The shell is pushed further due to the interaction of the wind with the characteristic magnetic field pattern (Fig. 4b). The radio polarization intensity distribution (Fig. 4d) forms a much less circular structure because of the projection effects. The map reveals one visible maximum on the same side as it is observed in model II (Fig. 4c). This field distribution better resembles the galaxy emission than the magnetic structures from model II, showing also larger depolarization region in the center. However, radial B-vectors in the central region of the galaxy are still not well reproduced. The uniformity of a shell configuration is present owing to the assumption of a smooth outflow distribution in the whole central area, whereas the wind is certainly connected with more locally distributed phenomena, e.g. star formation (see grayscale plot of $H\alpha$ emission Fig. 5d).

Our next reported experiment, model IV, takes into account all prior processes (i.e. turbulent diffusion, α -effect, presence of the outflow) and the random magnetic field component is added in the central part of the galaxy at every 10^7 yr. The resultant magnetic field configuration changes significantly, as is shown in Fig. 5a for the time step equal to $t=1.3 \times 10^8$ yr. The B-vectors, possessing high pitch angles, form a kind of a spiral shell-like structure with the intensity maximum distributed from the bottom to the top on the eastern side of the bar. Magnetic fields are weaker on the western side, diminishing significantly in its upper part. In contrast to our previous models, we can now observe chaotically distributed magnetic fields in the central bar regions, resulting from the seeded random component. These fields are elongated slightly by the wind into filaments going outwards the disk. Due to random field, outflow and the velocity shear the B-vectors start to form small region with B-vectors showing the opposite direction to the input magnetic field. The PI map of the presented model (Fig. 5b) especially in its periphery seems to be in a good agreement with observations. We have got a polarized shell with one maximum of emission at the western part of the modeled galaxy pattern (see Figs. 5b and d). At the bottom end of the bar, the polarized shell is slightly stronger than the observed one, however the distribution of pitch angles fits the observational one quite well (see Fig. 7). Also the Faraday rotation measure computed for this model gives quite good agreement with observations, as is presented in Fig. 7 (see discussion below). The magnetic field vectors in the central part show clear signs of flow outwards from the disk center (at the south-west part of the central part, Fig. 5a), but their PI presentations do not give the observed structure. This fact is obviously connected with the assumed outflow geometry and the involved distribution of random magnetic field component, which we plan to improve in future modeling.

Model V discusses the possibility of magnetic field origin due to such processes as stellar ejections, outflows and velocity shears but without the dynamo mechanism. In order to make the process of building up of the random component more vigorous, we assume that the averaged magnetic strength is five times higher than for model IV and we allow for longer evolution (for 9.0×10^8 yr). Such high mean value is still in agreement with a

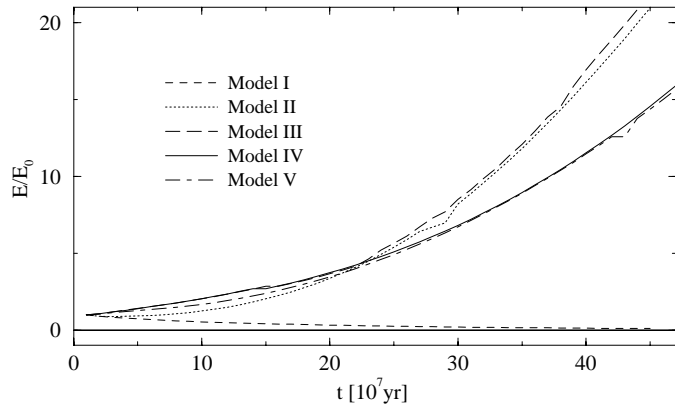


Fig. 6. The time evolution of the total magnetic energy E normalized to the initial energy E_0 for five models analyzed (see Table 2).

theoretical range (Ruzmaikin et al. 1988). The map of polarized emission from the modeled magnetic structure at the time step of 0.9×10^9 yr is presented in Fig. 5c. We see that magnetic field is distributed only in the central part of the modeled galaxy. The outer shell in this model has not been formed at all. The high degree of PI of the actual model (Fig. 5c) results from the assumed high intensity of the random component aligned along radial direction due to wind influence. The Faraday rotation measure computed for this map shows a chaotic distribution in opposition to model IV.

Fig. 6 presents the time evolution of a total magnetic energy (E) normalized to its initial value (E_0) for our five models. In three experiments (II–IV) taking into account the α -effect, the total energy grows, as expected, while in model I with no amplifications, it decreases. The energy in model V grows similarly to case IV because of the continuous supply of a substantially stronger random component in this experiment. Model III shows the highest increase due to a strong interaction of the wind with the shell-like structure of the magnetic field. In experiment IV the magnetic energy grows slower than in models II and III, due to a fast dispersion of the random component in the central region caused by the turbulent diffusion. The total magnetic energy (in cases II–V) increases several times, resulting in the maximum magnetic field values of about $7 \mu\text{G}$, which is in good agreement with observations.

To make quantitative comparison of the magnetic properties of NGC 4449 and our best model IV, we analyze distributions of the pitch angles of B-vectors and radio polarization intensity (PI) at 4.86 GHz, as well as Faraday rotation measures (RM) between 4.86 GHz and 8.46 GHz. As calculations are performed in arbitrary units, we adopt thermal electron density providing RM in the range consistent with observations. The comparison is made along a ring of $1'$ wide and having the same inclination and position angle as the galaxy (see Table 1). The ring extends from $2'$ to $3'$ from the centre and covers the magnetic shell-like structure. The values of all three distributions are averaged along the azimuthal angle in the plane of the galaxy, in sectors of 30° width. The azimuth is evaluated from the galaxy major axis and goes anti-clockwise. As seen in Fig. 7 the modeled distributions

of the pitch angle, PI and RM (dashed lines) possess quite similar character to the features observed in the galaxy (solid lines). For both, NGC 4449 and the model, the magnetic vectors are directed outward showing positive pitch angles over almost the whole range of the azimuthal angle. The pitch angles start from small values in the first sector and grow within the first quadrant to 60° . Then they decrease and increase again to the highest values about 75° in the third quadrant. As seen in Fig. 7 (the middle plot) the model PI distribution resembles that in NGC 4449, up to the angle about 270° , with maximums peaking in adjacent sectors. In the last region of the azimuthal angle, the galaxy PI values are higher than the modeled ones. This is probably due to a local enhancement of star formation in the northern part of the galaxy where the youngest population of star formation is observed and produces strong features in optical (see Fig. 3d), $H\alpha$ (Fig. 5d) and X-ray images. We also observe (Fig. 7, at the bottom) a qualitative agreement of the model with the observed distribution of RM. Both distributions show coherent areas with low positive RM (first quadrant) and higher RM with absolute values reaching locally $250\text{--}350\text{ rad/m}^2$. The highest discrepancies between RM distributions occur in sectors centred around the azimuthal angle of 120° and 180° , however in these sectors the highest statistical errors in the RM distribution of NGC 4449 are also observed (140 and 260 rad/m^2 , respectively). During computation of the average values of RM, the RM in the model was clipped in areas with no statistically significant signal in the observed Q and U maps of NGC 4449 (especially important for the lower sensitivity 8.46 GHz data). As a result, a gap in both RM distributions is seen.

6. Discussion and conclusions

A numerical model involving a three-dimensional flow of a molecular gas around a bar, is applied to study the kinematic evolution of a large-scale magnetic field of an irregular galaxy under the influence of three mechanisms: dynamo amplification, spherical outflow and a source of a chaotic magnetic field provided by active star-forming regions. We perform a comparison between resultant magnetic structures of a modeled galaxy with recent radio observations of NGC 4449. Our present work demonstrates that a regular large-scale magnetic field in irregular galaxies similar to NGC 4449 could be a result of a combined action of the aforementioned processes.

In order to model the observed velocity field of the NGC 4449 (Hartmann et al. 1986, Sabbadin et al. 1984, Hunter et al. 1998) we assume that the gas rotates slowly around the bar perturbation, with the maximum velocity value of 30 km s^{-1} , and possesses substantial velocity gradients (see Fig. 1 and 2). Both phenomena are observed in the real galaxy. In addition to the r.m.s velocity, we additionally introduce a spherical outflow of 50 km s^{-1} maximum velocity blowing from the central region of active star formation. The velocity field resulted from the N-body simulations (Otmianowska-Mazur et al. 1997) showing a bar structure, and recalculated to smaller velocity and scale values, is next used as an input parameter to the solution of the dynamo Eq. (1).

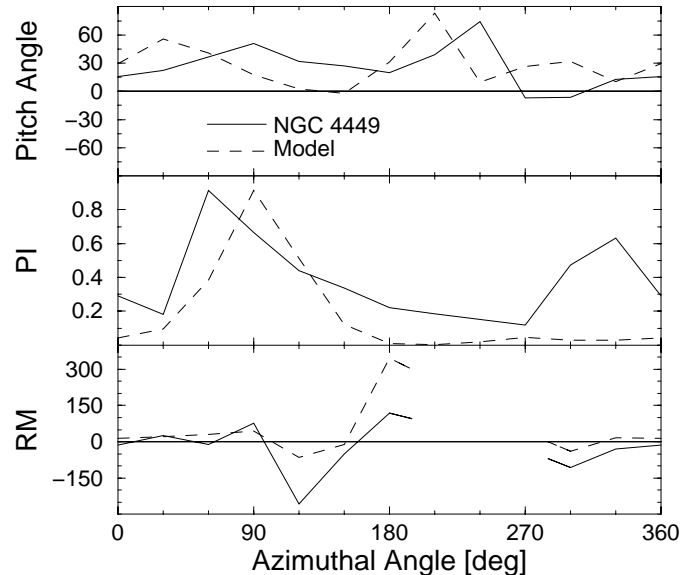


Fig. 7. The comparison of magnetic pitch angle (in deg), polarized intensity (PI, in arbitrary units) and Faraday rotation measures (RM, in rad/m^2) distributions of model IV and NGC 4449 in the outer ring around the galaxy center (see text).

Model I shows (Figs. 3a and c) that the magnetic field with no dynamo action forms a clearly visible ring of magnetic vectors around the bar. Inside this shell the magnetic field is quickly diffused due to fast changes of the radial velocity sign in this area (see Fig. 3b). The polarization map constructed from the simulation at time steps of $1.3 \cdot 10^8\text{ yr}$ (Fig. 3c), does not show good agreement with the observations (Fig. 3d), possessing too small pitch angles and uniformly distributed emission. The total magnetic energy decreases during the whole evolutionary time.

Inclusion of the dynamo process in our calculations causes an increase of the total magnetic energy, and of a local maximum magnetic strength from 1 to $7\ \mu\text{G}$ (as it is observed), as well as, significant reorganization of the modeled magnetic structures (Figs. 4a and c). The resulting map of a polarized emission (at the same time-step as in model I) possesses a non-uniform shell-like distribution, more similar to the observed patterns (Fig. 3d) than our previous calculations. The resultant pitch angles increase due to the dynamo action, giving values similar to NGC 4449.

The presence of the outflow enhances the magnetic strength in the ring, showing more clearly a shell pattern around the bar. The modeled flow is distributed uniformly around the galactic center, being quite different from the real outflows in NGC 4449, where they seem to be distributed instead along the galactic bar (according to $H\alpha$ map, Fig. 5d, greyscale plot). The resultant magnetic shell is pushed further (Fig. 4b) in comparison with model II (Fig. 4a), and due to the projection effects, the obtained PI map is even more similar to the emission of the observed galaxy than the structure obtained in computations II. The depolarized emission area appears in the central part of the modeled disk similarly to NGC 4449.

Model IV, which additionally combines a random magnetic field component provided by star formation regions, gives

the best estimation of the observed polarization distribution of NGC 4449 (Fig. 5b and d). The maps of modeled and observed galaxy are similar in the shell-like spiral patterns distributed in peripheries of both disks, which is evident by the pitch angle, PI and RM analysis (Fig. 7). The combination of all four processes: velocity shear around a bar, dynamo action, wind interaction and supplying the random magnetic field component, results in good agreement between modeled and observed polarization properties and configuration of fragments of a shell-like spiral pattern.

Model V (Fig. 5c) shows that the inclusion of a galactic spherical wind and recurrent production of chaotic magnetic fields in the central region of the galaxy does not result in the observed fan-like structures in the central part of the NGC 4449 nor in the fragments of a spiral large-scale structure in its peripheries.

The good correlation between the observed shell-like structure in HI and polarized radio shell (Chyży et al. 2000) could be related to the ring-like structures present in a large number of barred galaxies (Buta 1986, Hummel et al. 1987). Such rings are normally interpreted as concentrations of stars and gas developed near the Lindblad resonances. The observation of such a feature in NGC 4449 could confirm the hypothesis that the gas flow and the radio polarized shell in this galaxy is connected with the bar perturbation.

The highly asymmetrical character of the observed polarized emission of the Large Magellanic Cloud (Klein et al. 1993) indicates that magnetic field in this object is influenced by strong interaction with our Galaxy and possibly with the SMC (NGC 4449 is in this context more isolated). LMC has also three times smaller optical and radio brightness. In X-rays the total emission in the point source component as well as in the diffuse one is 5 times smaller than in NGC 4449 and is possibly scaled with masses of these objects (7 and $2 \times 10^{10} M_{\odot}$, respectively). A smaller rate of stellar activity distributed mainly in the compression region at the leading edge of LMC (giant 30 Doradus neighborhood) can result in a smaller overall activity of the dynamo process and higher overall asymmetry of observed PI distribution, with an enhancement at the side in the direction to our Galaxy. Therefore, our simulations which concentrated instead on NGC 4449, cannot be fully applied to the case of the LMC. However, in the LMC a patchy polarized shell-like pattern containing spiral magnetic fields, modeled in this work, is also observed. The magnetic pitch angles are high in more quiescent areas (as in NGC 4449) and low in the compression (SE) region where magnetic fields are aligned with the leading edge (see Fig. 2 in Klein et al. 1993). The rotation measures in the LMC are rather complex and, similarly to PI, the main features are connected with the disturbed SE part of the galaxy. In fact, the derived RM suggest a giant magnetized loop emerging out of the LMC plane towards our Galaxy. All such local features were not included in our simulations.

We have presented here the first attempt to model the kinematic MHD evolution of magnetic fields in an irregular galaxy. However, full MHD calculations and simulations of other irregulars are clearly needed.

We can summarise the main conclusions of our study as follows:

1. Irregular galaxies could possess regions with a regular component of a large-scale magnetic field;
2. The regular magnetic structure in IBm irregulars could be developed due to shear motions of interstellar gas connected with the bar perturbation and to the fast dynamo mechanism;
3. The existence of a large-scale configuration of magnetic field is possible even for small values of a galactic rotation ($v < 30 \text{ km s}^{-1}$);
4. The MHD dynamo process is necessary to produce large pitch angle values and to sustain the magnetic energy in the disk against the diffusion process;
5. Gas outflows from the active star-forming regions alone cannot be responsible for the large-scale magnetic field evolution in irregular galaxies of Magellanic type.

Acknowledgements. The authors wish to express their thanks to Prof. Marek Urbanik and Prof. Hugo van Woerden for their helpful comments and discussions. We are grateful to Dr. Dominik Bomans for providing us with his H α map. We are thankful to an anonymous referee for critical reading of the manuscript and suggestions concerning its improvement. A large part of the computations were made using the Convex-SPP machine at the Academic Computer Center “Cyfronet” in Kraków (grant no. KBN/C3840/UJ/011/1996 and KBN/SPP/UJ/011/1996). This work was partly supported by a grant from the Polish Committee for Scientific Research (KBN), grant no. PB 4264/P03/99/17

References

- Athanassoula E., 1992, MNRAS 259, 345
 Bajaja E., Huchtmeier W. K., Klein U., 1994, A&A 285, 385
 Brandenburg A., Donner K.J., Moss D., et al., 1993, A&A 271, 36
 Breitschwerdt D., McKenzie J.F., Völk H.J., 1991, A&A 245, 79
 Bomans D., Chu Y.-H., Hopp U., 1997, AJ 113, 1678
 Buta R., 1986, ApJS 61,609
 Chyży K., Beck R., Kohle S., Klein U., Urbanik M., 2000 A&A 355, 128
 de Boer K.S., Braun J.M., Vallenari A., Mebold U., 1998, A&A 329,L49
 de Vaucouleurs G., de Vaucouleurs A., Corwin H., 1976, Second Reference Catalogue of Bright Galaxies, Austin: Univ. of Texas
 de Vaucouleurs G., de Vaucouleurs A., Corwin H., et al., 1991, Third Reference Catalogue of Bright Galaxies, New York: Springer
 Elstner D., Meinel R., Beck R., 1992, A&AS, 94, 587
 Elstner D., Lesch H., von Linden S., Otmianowska-Mazur K., Urbanik M., 1998, Studia geophysica & geodetica 3, 373
 Hanasz M., 1997, A&A 327, 813
 Hanasz M., Lesch H., 1997, A&A 321, 1007
 Hanasz M., Lesch H., 1998, A&A 339, 629
 Hartmann L., Geller M., Huchra J., 1986, AJ 92, 1278
 Hill R., Home A., Smith A., et al., 1994, ApJ 430, 568
 Hummel E., van der Hulst J., Keel W., 1987, A&A 172,32
 Hunter D., Gallagher J., 1990, ApJ 362, 480
 Hunter D., Gallagher J., 1992, ApJ 391, L9
 Hunter D., Wilcots E., van Woerden H., Gallagher J., Kohle S., 1998, ApJ 495, L47
 Klein U., Haynes R., Wielebinski R., Meinert D., 1993, A&A 271, 402

- Klein U., Hummel E., Bomans D., Hopp U., 1996, A&A 313, 396
- ♣ Meinel R., Elstner D., Rüdiger G., 1990, A&A 236, L33
- Luks T., Rohlf's K., 1992, A&A 263, 41
- Otmianowska-Mazur K., von Linden S., Lesch H., Skupniewicz G., 1997, A&A 323, 56
- Pacholczyk, 1970, Radio Astrophysics. Nonthermal Processes in Galactic and Extragalactic Sources., San Francisco: W.H. Freeman Co.
- Parker E., ApJ 1992, 401, 137
- Pohl M., Schlickeiser R., 1990, A&A 239, 424
- Rädler K.-H., Wiedemann E., GAFD, ♣(1989?), 49, 71
- ♣ Rüdiger G., 1990, GAFD 50, 53
- Ruzmaikin A., Shukurov A., Sokoloff D., 1988, Magnetic Fields of Galaxies, Dordrecht: Kluwer
- Sabbadin F., Ortolani S., Bianchini A., 1984, A&A 131, 1
- Stone J., Norman M., 1992, ApJS 80, 791
- Tully R., 1988♣, Nearby Galaxies Catalog, Cambridge: Cambridge University Press
- van Woerden H., Bosma A., Mebold U., 1975, In: Weliachew L. (ed.), La Dynamique des Galaxies Spirales, Paris: Edition du CNRS, p. 483
- ♣ von Linden S., Otmianowska-Mazur K., Lesch H., Skupniewicz G., 1998, A&A 333, 79
- Westerlund B., ♣(1990?), A&A Rev. 2, 29